J Mater Sci (2010) 45:1448–1452
DOI 10.1007/s10853-009-4099-y

Preparation of $SrTiO_3$ nanomaterial by a sol–gel-hydrothermal method

S. Fuentes · R. A. Zarate · E. Chavez · P. Muñoz · D. Díaz-Droguett · P. Leyton

Received: 13 July 2009 / Accepted: 30 November 2009 / Published online: 15 December 2009

Abstract A new synthetic route to obtain high-purity strontium titanate, $SrTiO_3$, using the sol–gel-hydrothermal reaction of $TiCl_4$ and a $SrCl_2$ solution in an oxygen atmosphere has been developed. In the synthesized products the $SrTiO_3$ nanoparticles are nearly spherical and decrease in size with the reaction time (48 h) down to a diameter of about 40 nm. The microstructure and composition of the as-synthesized samples were investigated by X-ray diffraction (XRD), high-resolution TEM (HRTEM), Raman spectroscopy, atomic force microscopy (AFM), and energy-dispersive X-ray spectroscopy (EDX). All the samples were identified as cubic perovskite phase.

Introduction

Ferroelectric oxides such as $BaTiO_3$ and $SrTiO_3$ with a perovskite structure are widely used in the fields of nonlinear optics, pyroelectric detectors, electro-optical modulators, thin-film capacitors, and optical memories [1, 2]. Strontium titanate ($SrTiO_3$) is a well-known cubic-perovskite-type paraelectric oxide with a large nonlinear optical coefficient and high dielectric constant, thermal stability, and photocatalytic properties [3, 4]. However, because its properties are dependent not only on its chemical composition but also on its structure, shape, and size [5, 6], it has been found that reduction of the grain size of $SrTiO_3$ to the nanoscale leads to distinct properties from those of the bulk [7, 8]. The ability to tune the size and shape of $SrTiO_3$ particles is significant for fundamental studies as well as for preparing ceramics and composite materials with tailored properties.

The traditional preparation methods of perovskite-type powders are in the solid state at high temperatures, usually >900 °C, and sol–gel techniques that involve extreme temperature, pressure, and pH conditions [9, 10]. On the other hand, several techniques are available for synthesizing fine strontium titanate powders. These include a chemical solution process [11], sol–gel methods [12], thermal decomposition of mixed citrate or oxalate complexes [13], hydrothermal methods [14], and freeze drying of nitrate solutions [15].

In recent years, some new methods have been introduced to make porous $SrTiO_3$. These methods include the development of soft-chemistry routes to produce nanoparticles or specially shaped materials such as one-dimensional nanowires [16–18], sonochemical methods to prepare size-tunable strontium titanate crystals [19], and the inverse micelle microemulsion method to prepare $SrTiO_3$ nanopowders [20]. Among these various synthetic methods, hydrothermal or chemical reaction methods are of great interest because they are safe and environmentally friendly synthesis performed at moderate temperatures (around 200 °C) and they are effective methods for

S. Fuentes (✉) · R. A. Zarate · E. Chavez
Departamento de Física, Facultad de Ciencias, Universidad Católica del Norte, Casilla 1280, Antofagasta, Chile
e-mail: sfuentes@ucn.cl

P. Muñoz
Departamento de Química, Facultad de Ciencias, Universidad Católica del Norte, Casilla 1280, Antofagasta, Chile

D. Díaz-Droguett
Departamento de Física, Facultad de Ciencias Físicas y Matemáticas, Universidad de Chile, Casilla 487-3, Santiago, Chile

P. Leyton
Laboratorio de Fotofísica y Espectroscopia Molecular, Instituto de Química, Pontificia Universidad Católica de Valparaíso, Av. Brasil N:2950, Valparaíso, Chile

creating novel architectures or hierarchical structures based on nanocrystals [21].

In the present article we report a new route to directly synthesize cubic highly nanocrystalline $SrTiO_3$ powder using $TiCl_4$ and $SrCl_2$ as starting materials by the sol–gel-hydrothermal method in an oxygen atmosphere.

Experimental section

In a typical procedure, 1.1 mL of $TiCl_4$ was diluted with 2.3 mL of 2 M HCl to form a yellowish solution, and $Sr(OH)_2{\cdot}8H_2O$ was dissolved in 40 mL of deionized water. The two solutions were mixed to form strontium titanium solution. With stirring and N_2 bubbling, 13 mL of 6 M NaOH was added to the strontium titanium solution, forming a white homogeneous colloidal strontium titanium slurry. The mixed solution was transferred into a 500 mL Teflon-lined stainless steel reactor, sealed, and then heated at 180 °C and kept for 12–48 h under an oxygen partial pressure of 60 psi. At the end of the reaction the autoclave was allowed to cool to room temperature. The as-synthesized white powder that attached to the bottom and inner wall of the Teflon container was collected, centrifuged, washed with distilled water and ethanol to remove the remaining ions, and dried at 60 °C for 6 h under reduced pressure.

The XRD data were recorded on a Siemens D5000 diffractometer with Cu K_α radiation (40 kV, 30 mA). The morphology of the samples was examined using Low Vacuum Scanning Electron Microscopy (LV-SEM, JSM-6360LV) equipped with an EDX detector. Transmission electron microscopy (TEM) studies were made on a Tencai F20 FEG-TEM operated at 200 kV equipped with an EDS detector. The samples were ultrasonically dispersed in ethanol and later they were collected on a carbon grid for TEM examination. The Raman spectra were recorded on a WITEC model CRC200 using a 5.5-mW laser with a wavelength of 514.5 nm. The morphology also was studied by atomic force microscopy, using a WITEC AFM model Mercury 100.

Results and discussion

In Fig. 1 is shown the XRD patterns of the samples obtained at 180 °C at an oxygen partial pressure of 60 psi and reaction times of 12–48 h. All the products, obtained at different reaction times, have almost the same XRD patterns. The peaks exhibited can be indexed as cubic lattice (space group *Pm3m*) of $SrTiO_3$ and the calculated lattice constants are in good agreement with the tabulated values ($a = 3.1912$ Å; JCPDS cards no. 73-0661). By comparing

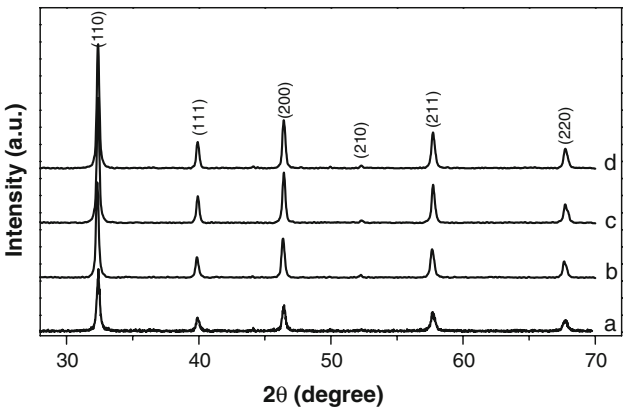

Fig. 1 XRD patterns of the product obtained at 180 °C after different reaction times: (*a*) 12 h, (*b*) 24 h, (*c*) 32 h, and (*d*) 48 h

to the standard XRD pattern of the $SrTiO_3$ powder, the peaks at 32.4°, 39.9°, 46.4°, 52.2°, 57.7°, and 67.8° can be attributed to the Miller indices of (110), (111), (200), (210), (211), and (220). In the [110] plane of $SrTiO_3$ were calculated the values of full width at half maximum (FWHM), which were of 3.962×10^{-3} and 4.608×10^{-3} for samples with 12 and 48 h of reaction, respectively. Also, we calculated the average particle sizes and the values were of 54 and 46 nm for samples treated by 12 and 48 h, respectively. For this estimation we supposed that geometry of the particles is spherical. Therefore, the particle size decreases with the reaction time.

In Fig. 2 the Raman spectra of the $SrTiO_3$ powder after reaction periods of 12 and 48 h is depicted. There are four photon lines at around 185, 340, 549, and 798 cm^{-1} that are ascribed to TO_2, TO_3, TO_4, and LO_4 first-order modes,

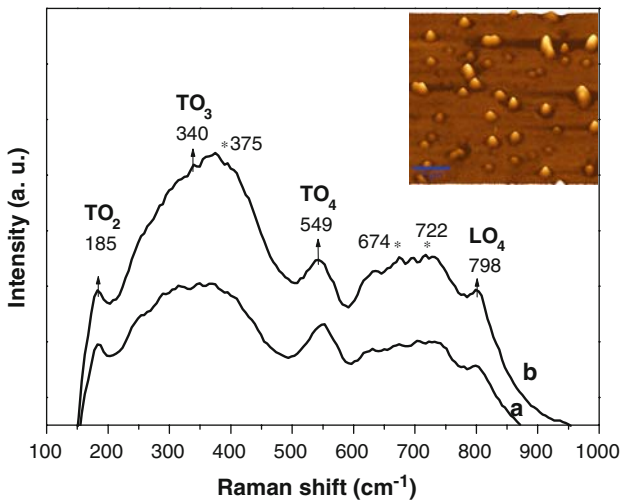

Fig. 2 Raman spectra of the product obtained at different reaction times: (*a*) 48 h, (*b*) 12 h. The *inset* shows a Raman image of $SrTiO_3$ nanoparticles obtained at 48 h

respectively, while the intensities of the bands ascribed to the second-order modes at 337, 674, and 722 cm^{-1} decrease, as the particle size decreases. This decrease is greater in samples treated for 48 h (Fig. 2a) than previous samples. In the inset the Raman image of $SrTiO_3$ nanoparticles obtained at 48 h is shown.

However, $SrTiO_3$ single crystals at room temperature have an ideal cubic perovskite structure (space group *Pm3m*) and the vibration modes are $3F1u + F2u$ [22]. *F2u* and *F1u* are not modes Raman active in which the first-order Raman scattering is symmetrically forbidden in bulk $SrTiO_3$. However, studies of the Raman spectra of $SrTiO_3$ have shown that first-order Raman scattering can be observed. This occurs when the central symmetry is broken due to many factors such as strain effects, the presence of impurities and defects, oxygen vacancies, and even external conditions [23–25]. Recently, Wu et al. [6] observed the effect of size in $SrTiO_3$ nanoparticles by Raman spectroscopy and found that with further particle size reduction, the intensities of the first-order modes (TO_2 and TO_4) increase, while those of most of the second-order modes show a gradual decrease.

Morphology was also analyzed by atomic force microscopy and the results indicated the particles are almost spherical shape, as shown in Fig. 3. The particle size distribution histograms are shown at the bottom left corners of corresponding AFM images. Average particle size was estimated from AFM images taken by acoustic or tapping mode, the results were 105 and 70 nm for the samples treated at 12 and 48 h, respectively. The average particle sizes estimated by AFM images are larger than those calculated by Debye-Scherer formula.

Transmission electron microscope (TEM) and high-resolution transmission electron microscope (HRTEM) images provide an insight into the structure of the $SrTiO_3$ prepared at 48 h as shown in Fig. 4, where the bright-field TEM image under low magnification reveals that the $SrTiO_3$ nanoparticles are nearly spherical with a diameter range of 35–46 nm, as you can see in Fig. 4a. This particle size is complete agreement with the calculated value with Debye-Scherer formula, which was about 46 nm. It is well-known that in the perovskite structure the [110] planes have the lowest surface energy, and in turn they have the lowest planar growth rate, thereby making the equilibrium phase cubic as seen in other perovskites [26]. On the other hand, the strain associated with the stabilization of the cubic structure tends to reduce the surface area of the growing particles, which retain a spherical morphology. In the HRTEM image at Fig. 4b is shown that the regular spacing of the observed lattice planes was about 0.238 and 0.269 nm, which are, respectively, consistent with the [111] and [110] lattice spacing of cubic $SrTiO_3$ nanoparticles. Their corresponding SAED pattern shown in Fig. 4c displays a polycrystalline diffraction ring composed of discrete diffraction spots, indicating the crystalline nature of the nanoparticles. In Fig. 4d the EDX result shows that the sample only contains the elements Sr, Ti, and O.

The elemental composition and oxidation states of the samples that were analyzed by X-ray photoelectron spectroscopy are shown in Fig. 5. The position of the Sr 3d-doublet lines (Fig. 5a) at 132.9 and 134.5 eV are attributed to Sr $3d_{5/2}$ and the peak at 18.9 eV is attributed to the shake up (Fig. 5b). The positions of the Ti $2p_{3/2}$, Ti $2p_{1/2}$, and its satellite peak are shown in Fig. 5c and are located at 458.4, 463.8, and 471.9 eV, respectively. The binding energy and the satellite position (marked 1) are consistent with those of a Ti ion in the perovskite titanate of Sr. As shown in Fig. 5d, the O 1s core-level spectrum is broad, and two Gaussians were resolved using a curve-fitting procedure. The O 1s peak position of ~529 eV is a typical value for oxygen in perovskites [27]. This indicates that the oxygen ions remain coordinated in TiO_6 octahedra. A peak 2 at higher energies of 531.7 eV is associated with OH groups and with water absorbed onto the surface of the $SrTiO_3$.

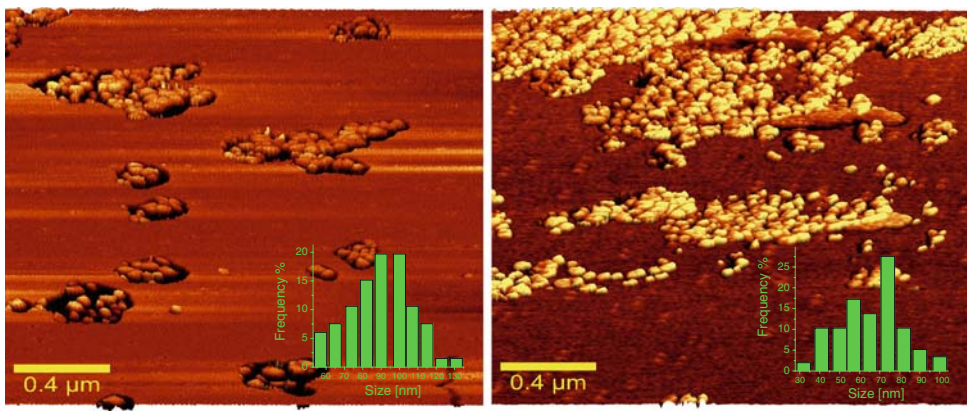

Fig. 3 Acoustic AFM images of $SrTiO_3$ nanoparticles obtained at: **a** 12 h and **b** 48 h. The *insets* are their corresponding particle size distribution histograms

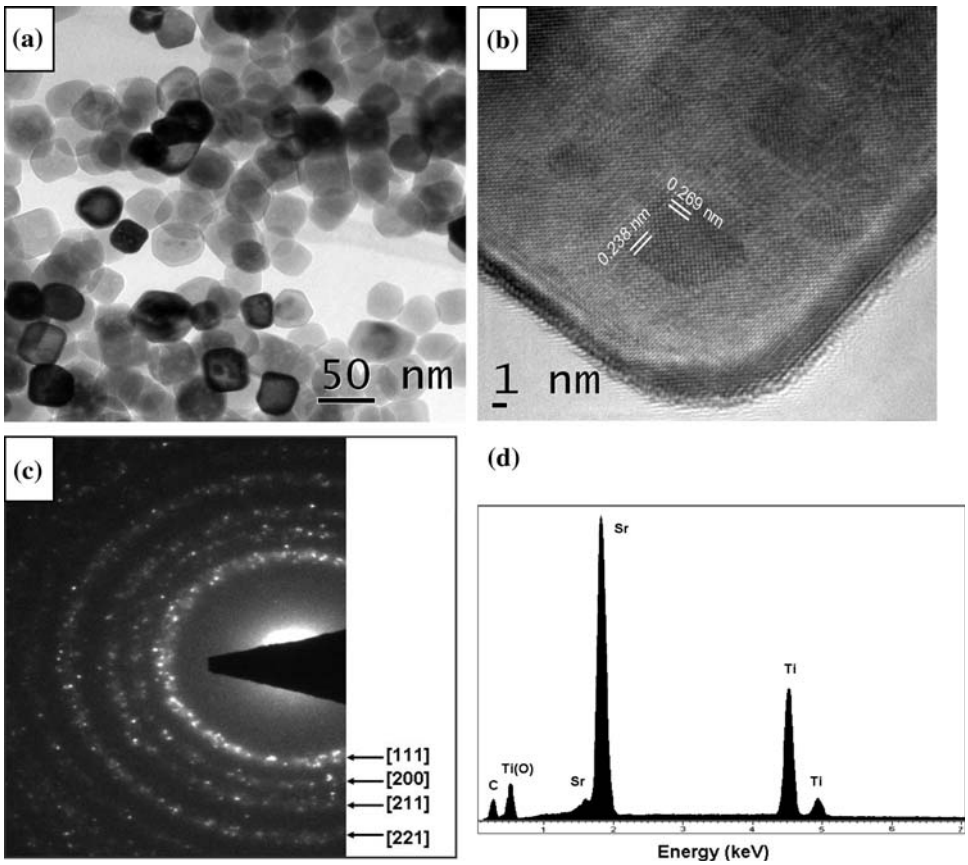

Fig. 4 Morphology and structure of the $SrTiO_3$ nanoparticles obtained at 48 h. **a** TEM image, **b** HRTEM image, **c** SAED pattern, and **d** corresponding EDX

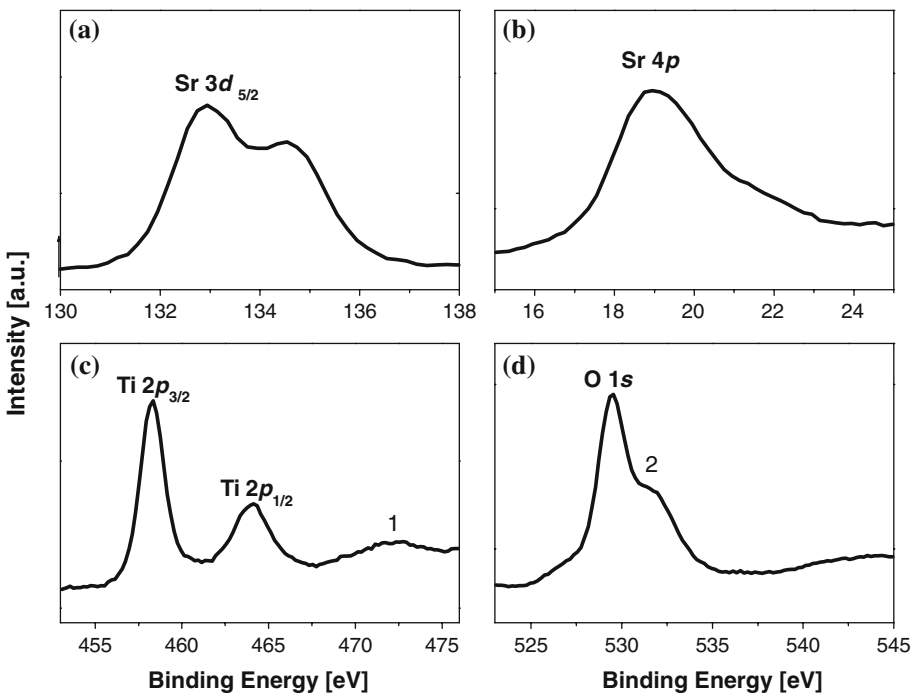

Fig. 5 XPS spectra of the $SrTiO_3$ nanospheres prepared hydrothermally for 48 h. Spectra **a** Sr 3d doublet, **b** valence band spectra Sr 4p, **c** Ti $2p_{3/2}$, **d** O 1s

Conclusion

In summary, on the basis of AFM, XRD, XPS, SEM, TEM, and Raman spectroscopy, we have successfully synthesized and shape-controlled $SrTiO_3$ crystallites by a sol–gel-hydrothermal method under an oxygen partial pressure of 60 psi. We proved that the particle size decreases with the reaction time. At 180 °C, the $SrTiO_3$ nanoparticles are nearly spherical and their size decreased from 70 nm up to a diameter of about 40 nm with reaction times from 12 h up to 48 h, respectively. The growth mechanism of the controlled shape $SrTiO_3$ is suggested as a shape evolution resulting from the faster growth rate along the [110] direction of the $SrTiO_3$ cubic lattice.

Acknowledgements This work has been partially financed by FONDECYT Grant under contract No 1080401. The authors thank the Facultad de Ciencias Físicas y Matemáticas of the Universidad de Chile for the use of their analytical equipment (XRD, TEM, and XPS). R.A.Z. acknowledges FUNDACION ANDES Grant under contract No C-13876.

References

1. Hill N (2000) J Phys Chem B 104:6694
2. Schrott A, Misewich J, Nagarajan V, Ramesh R (2003) Appl Phys Lett 82:4770
3. Luo J, Maggard P (2006) Adv Mater 18:514
4. Liu J, Chena G, Lia Z, Zhang Z (2006) J Solid State Chem 179:3704
5. Rudiger A, Schneller T, Roelofs A, Tiedke S, Schmitz T, Waser R (2005) Appl Phys A 80:1247
6. Wu X, Wu D, Liu X (2008) Solid State Comm 145:255
7. Zhang W, Yin Z, Zhang M (2000) Appl Phys A 70:93
8. Kwun SI, Song TK (1997) Ferroelectrics 197:125
9. Hernandez B, Chang K, Fisher E, Dorhout P (2002) Chem Mater 14:480
10. Mao Y, Banerjec S, Wong S (2003) J Am Chem Soc 125:15718
11. Dedyk A, Karmanenko S, Leppavuori S, Sakharov V (1998) J Phys Fr 8:217
12. Hou B, Xu Y, Wu D, Sun Y (2006) Powder Technol 170:26
13. Sekar M, Dhanaraj G, Phat H, Patil K (1992) J Mater Sci Mater Electron 3:237
14. Xu H, Wei S, Wang H, Zhu M, Yu R, Yan H (2006) J Cryst Growth 292:159
15. McHale J, McIntyre P, Sickafus K, Coppa N (1996) J Mater Res 11:1199
16. Khollam Y, Potdar H, Deshpande S, Gaikwad A (2007) Mater Chem Phys 97:295
17. Xie J, Ji T, Yang X, Xiao Z, Shi H (2008) Solid State Commun 147:226
18. Mao-yu T, Tian-hao J, Jian X (2007) Chin J Aeronaut 20:177
19. Demirors A, Imhof A (2009) Mater Chem. doi:10.1021/cm900693r
20. Su K, Nuraje N, Yang N (2007) Langmuir 23:11369
21. Yoshimura M (1998) J Mater Res 13:796
22. Venkateswaran U, Naik V, Naik R (1998) Phys Rev B 58:14256
23. Du Y, Chen G, Zhang M (2004) Solid State Commun 130:577
24. Kleemann W, Albertini A, Kuss M, Linder R (1997) Ferroelectrics 203:57
25. Akimov I, Sirenko A, Clark A, Hao J, Xi X (2000) Phys Rev Lett 84:4625
26. Liu X, McCandlish E, McCandlish L, Bolen K, Ramesh R, Cosandey F, Rossetti G, Riman R (2005) Langmuir 21:3207
27. Ehre D, Cohen H, Lyahovitskaya V, Lubomirsky I (2008) Phys Rev B 77:184106